ACS APPLIED MATERIALS & INTERFACES

Research Article

www.acsami.org

From Water Oxidation to Reduction: Transformation from $Ni_xCo_{3-x}O_4$ Nanowires to NiCo/$NiCoO_x$ Heterostructures

Xiaodong Yan,[†] KeXue Li,[§] Lu Lyu,[‡] Fang Song,[∥] Jun He,[‡] Dongmei Niu,[‡] Lei Liu,[§] Xile Hu,[∥] and Xiaobo Chen*[,†]

[†]Department of Chemistry, University of Missouri−Kansas City, Kansas City 64110, Missouri United States

[‡]School of Physics and Electronics, Hunan Key Laboratory for Super-microstructure and Ultrafast Process, Central South University, 932 South Lushan Road, Changsha, Hunan 410083, China

[§]State Key Laboratory of Luminescence and Applications, Changchun Institute of Optics, Fine Mechanics and Physics, Chinese Academy of Sciences, Changchun, 130033, China

[∥]Ecole Polytechnique Fédérale de Lausanne (EPFL), Institute of Chemical Sciences and Engineering, EPFL-SB-ISIC-LSCI, bch 3350, Lausanne CH 1015, Switzerland

Supporting Information

ABSTRACT: A homologous Ni−Co based nanowire catalyst pair, composed of $Ni_xCo_{3-x}O_4$ nanowires and NiCo/$NiCoO_x$ nanohybrid, is developed for efficient overall water splitting. $Ni_xCo_{3-x}O_4$ nanowires are found as a highly active oxygen evolution reaction (OER) catalyst, and they are converted into a highly active hydrogen evolution reaction (HER) catalyst through hydrogenation treatment as NiCo/$NiCoO_x$ heteronanostructures. An OER current density of 10 mA cm^{-2} is obtained with the $Ni_xCo_{3-x}O_4$ nanowires under an overpotential of 337 mV in 1.0 M KOH, and an HER current density of 10 mA cm^{-2} is obtained with the NiCo/$NiCoO_x$ heteronanostructures at an overpotential of 155 mV. When integrated in an electrolyzer, these catalysts demonstrate a stable performance in water splitting.

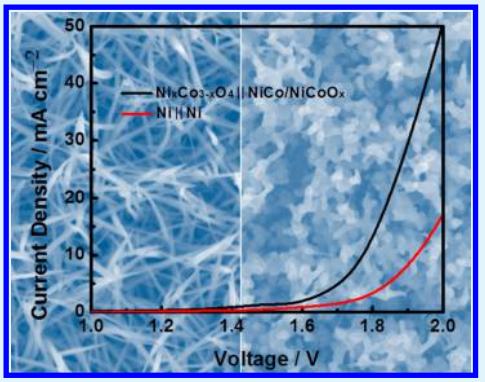

KEYWORDS: *nickel cobalt oxide, nanowires, metal/metal oxide heterostructures, hydrogen evolution reaction, oxygen evolution reaction*

1. INTRODUCTION

Water splitting through photocatalysis and electrolysis has attracted huge attention,[1−4] as hydrogen is a highly desirable energy carrier for future clean and renewable energy supply. Over the past several years, water splitting through photocatalysis has made great breakthrough, especially owing to the discovery of various black titanium dioxide nanomaterials through hydrogenation treatment.[1,5,6] Although remarkably enhanced hydrogen generation rate was observed in black titanium dioxide,[1] hydrogen production through photocatalysis is still far from practical applications due to its low efficiency. On the other hand, sustainable hydrogen production on a large scale can be achieved by water electrolysis using electricity from solar and wind energy.[7,8] The key to water splitting through electrolysis is the electrocatalysts. The state-of-the-art catalysts for hydrogen evolution reaction (HER) and oxygen evolution reaction (OER) are platinum and noble metal oxides (e.g., IrO_2 and RuO_2), respectively. However, their scarcity and high cost largely restrict their widespread applications.[9−13] Therefore, exploring the earth-abundant, low-cost electrocatalysts with high activity toward HER and/or OER is of significant importance.

Over the past decade, earth-abundant transition metals (especially Fe, Co, and Ni) and their derivatives have attracted tremendous attention. The discovery of new compounds contributed greatly to the development of earth-abundant, low-cost electrocatalysts. For example, transition metal phosphides[9,14−17] and transition metal layered double hydroxides[12,13,18−20] presented high catalytic activity for HER and OER, respectively. Another efficient way to achieve high-activity catalysts is to modify the structure of the existing materials. For instance, metal/metal oxide/carbon composites synthesized through carbon thermal reduction have been reported to possess much higher activity toward HER than the pristine metal/carbon composites.[21,22] Another example is electrochemical tuning, which can effectively tune the electronic structure of the materials for a better catalytic activity.[11,23−26] Recently, modification of metal oxides through hydrogenation treatment opens a new avenue to tune the catalytic activity of the metal oxide materials.[3,27,28] For example, Co/Co_3O_4 hybrid

Received: November 6, 2015
Accepted: January 19, 2016
Published: January 19, 2016

DOI: 10.1021/acsami.5b10724
ACS Appl. Mater. Interfaces 2016, 8, 3208−3214

nanosheets synthesized though hydrogenation achieved a benchmark current density of 10 mA cm^{-2} at a small overpotential of 90 mV in 1.0 M KOH,[3] and $WO_{2.9}$ derived from WO_3 through hydrogenation reached 10 mA cm^{-2} at a small overpotential of 70 mV in 0.5 M H_2SO_4.[28] More importantly, the catalytic activity is highly tunable by controlling the hydrogenation condition.[3,27]

Herein, we report on a homologous Ni−Co based nanowire pair composed of $Ni_xCo_{3-x}O_4$ nanowires and $NiCo/NiCoO_x$ hybrid nanowires as efficient electrocatalysts for overall water splitting. $Ni_xCo_{3-x}O_4$ nanowires as OER catalysts have been synthesized by hydrothermal reaction, and were converted into $NiCo/NiCoO_x$ heterostructural HER catalysts through hydrogenation treatment. The $Ni_xCo_{3-x}O_4$ nanowires exhibit a good OER activity with a small overpotential (337 mV) to reach a current density of 10 mA cm^{-2}. The $NiCo/NiCoO_x$ heterostructures present a markedly high HER activity with an overpotential of 155 mV to reach a current density of 10 mA cm^{-2}. Further, we investigated the overall water splitting performance of the electrolyzer with $Ni_xCo_{3-x}O_4$ as the anode electrode and $NiCo/NiCoO_x$ as the cathode electrode. A current density of 10 mA cm^{-2} was achieved at a voltage of 1.75 V in 1.0 M KOH, and the electrolyzer shows robust stability, thus suggesting an efficient, low-cost, earth-abundant electrode system for water splitting.

2. EXPERIMENTAL SECTION

2.1. Material Synthesis. In a typical synthesis, 0.25 mmol $Ni(NO_3)_2{\cdot}6H_2O$, 0.25 mmol $Co(NO_3)_2{\cdot}6H_2O$ and 2.5 mmol urea were dissolved in 16 mL deionized water as the precursor solution. A piece of nickel foam (~7 cm^2) was sonicated in 3 M HCl for 10 min to remove the possible surface oxide layer. After being washed with deionized water, the nickel foam was transferred into the precursor solution and reacted in a Teflon lined stainless steel autoclave at 120 °C for 12 h (hydrothermal process). After the reaction, the nickel foam was washed with deionized water and dried in air, followed by annealing at 300 °C for 2 h to obtain a $Ni_xCo_{3-x}O_4$ coated Ni foam. The sample was then treated in a hydrogen atmosphere at 250 °C for 3 h (hydrogenation) to obtain $NiCo/NiCoO_x$ nanohybrids-covered Ni foam. The mass loading of the $NiCo/NiCoO_x$ nanohybrids on nickel foam was about 0.7 mg cm^{-2}. To investigate the structure and composition of the $NiCo/NiCoO_x$ nanohybrids, we also applied similar processes to the powders formed in the hydrothermal process.

2.2. Property Characterization. Morphologies of the samples were examined using scanning and transmission electron microscopy (SEM and TEM). The SEM images were taken on a Hatachi 4700 field emission scanning electron microscope (FESEM). The foams were directly mounted on the sample stage for analysis. The TEM study was performed on a FEI Tecnai F20 STEM. The electron accelerating voltage was 200 kV. A small amount of powder sample dispersed in water was dropped onto a thin holey carbon film, and dried overnight before TEM measurement. Structural and chemical properties were studied with X-ray diffraction (XRD) and X-ray photoelectron spectroscopy (XPS). The XRD was performed using a Rigaku Miniflex X-ray diffractometer using Cu Kα radiation (wavelength = 1.5418 Å). XPS data were collected using a Kratos Axis 165 X-ray photoelectron spectrometer. Spectra were acquired using a photon beam of 1486.6 eV, selected from an Al/Mg dual-anode X-ray source. Fourier transform infrared (FTIR) spectra were recorded on a Thermo-Nicolet iS10 FT-IR spectrometer with an attenuated total reflectance unit.

2.3. Electrochemical Characterization. Electrochemical measurements were carried out in a three-electrode system at room temperature. A Pt wire and an Ag/AgCl electrode were used as the counter and reference electrode, respectively. 1.0 M KOH solution was used as the electrolyte. Cyclic voltammetry was performed five cycles in the voltage range of 0−0.5 V vs Ag/AgCl at a scan rate of 5 mV s^{-1} to activate the working electrode of the as-prepared samples. To prepare the IrO_2 electrode, IrO_2 (5 mg, 99%) were dispersed in mixed solvent of deionized water (1 mL) and 2-propanol (0.25 mL) via sonication for 0.5 h. Nafion solution (10 μL, 5 wt %) was added to increase the binding strength before sonication. Then, 35 μL of the suspension was drop-casted on Ni foam by micropipette, and the solvent was allowed to be evaporated at 70 °C for around 10 min. The catalyst loading was 0.7 mg cm^{-2}. Cyclic voltammetry was performed 30 cycles between 0.4 and 0.55 V vs Ag/AgCl at a scan rate of 10 mV s^{-1} until the oxygen evolution current of the IrO_2 electrode showed negligible change. Linear sweep voltammetry was conducted at a scan rate of 5 mV s^{-1} to evaluate the HER and/or OER performances of the all working electrode. Electrochemical impedance spectroscopy (EIS) analysis was performed using a 10 mV amplitude AC signal over a frequency range from 100 kHz to 10 mHz on a Biologic potentiostat/EIS electrochemical workstation. The polarization curve was *iR*-corrected for an ohmic drop obtained from EIS Nyquist plot. The reference electrode was calibrated with respect to reversible hydrogen electrode (RHE). The calibration was performed in a high purity hydrogen saturated 1 M KOH electrolyte with a Pt wire as the working electrode.

3. RESULTS AND DISCUSSION

The crystal structures of the resultant products were investigated by XRD. Figure S1 shows the XRD patterns of $Ni_xCo_{3-x}O_4$ and $NiCo/NiCoO_x$. The XRD pattern of the $Ni_xCo_{3-x}O_4$ nanowires obtained by reaction of 0.25 mmol Ni^{2+} and 0.25 mmol Co^{2+} at 120 °C for 12 h in the presence of urea matched well with the standard XRD pattern of Co_3O_4 (JCPDS 42-1467). After hydrogenation, the feature peaks of NiCo alloy at θ = 44.10, 51.62, and 76.08° match well with the (111), (200) and (220) characteristics of a face-centered cubic (fcc) NiCo structure, respectively, which is very similar to those of either fcc Ni (JCPDS 15-0806) or fcc Co (JCPDS 01-1260) while a slight variation for the peak position can be observed (all the peak positions lie between those of fcc Ni and fcc Co.). The average grain size was calculated using Scherrer's equation: $d = (k\lambda)/(\beta\cos\theta)$, where k is the shape factor with a typical value of 0.9, λ is the X-ray wavelength, β is the full width at half-maximum, θ is the Bragg angle, and d is the grain size.[3,27,29] The calculated average grain sizes of $Ni_xCo_{3-x}O_4$ and NiCo alloy were about 6 and 9 nm, respectively.

The morphology and detailed structures of the products were studied by SEM and TEM. SEM measurements showed that the Ni foam was fully covered by $Ni_xCo_{3-x}O_4$ nanowires (Figures S2 and S3), and was still fully covered by $NiCo/NiCoO_x$ nanohybrid after hydrogenation (Figures S4 and S5). The as-prepared $Ni_xCo_{3-x}O_4$ nanowires have an average diameter of ~20 nm and a length of more than 500 nm (Figure 1A). After hydrogen reduction, the morphology was altered due to the reduction and fusion, and thus the $NiCo/NiCoO_x$ nanohybrid had a nanorod-like morphology (Figure 1B). The TEM image in Figure 1C confirmed the nanorod-like morphology of the $NiCo/NiCoO_x$ nanohybrid. Figures 1D showed the HRTEM images of the $NiCo/NiCoO_x$ nanohybrid. A core−shell structure was revealed. The core features lattice fringes with the lattice spacing of 0.204 nm (inset, Figure 1D) corresponding to the (111) plane of face-centered cubic NiCo crystals.[30] The shell was mainly amorphous and had a thickness of 2−4 nm as indicated by the dotted line in Figure 1D.

The XPS survey of both $Ni_xCo_{3-x}O_4$ and $NiCo/NiCoO_x$ were shown in Figure 2A. The spectra were similar: signals from Ni, Co and O elements were observed with C deposition from the atmosphere. All the spectra were calibrated with the C 1s peak to 284.6 eV. Figure 2B shows the Ni 2p core-level XPS

DOI: 10.1021/acsami.5b10724
ACS Appl. Mater. Interfaces 2016, 8, 3208−3214

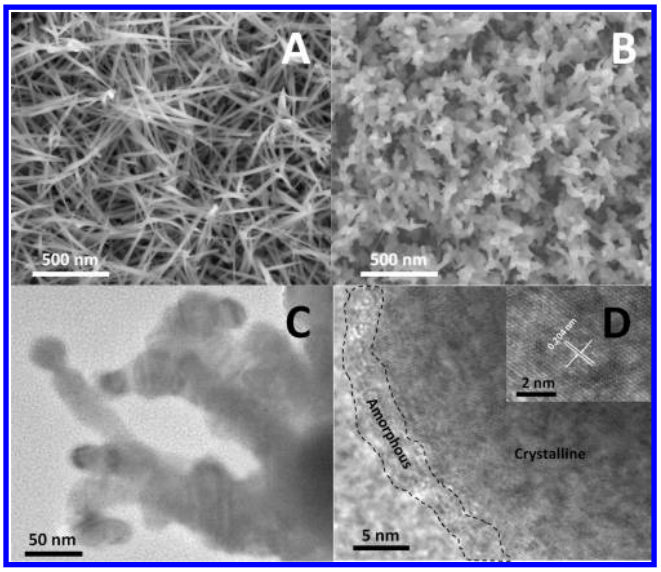

Figure 1. SEM images of (A) $Ni_xCo_{3-x}O_4$ nanowires and (B) NiCo/$NiCoO_x$ nanohybrid. (C) Low-resolution and (D) high-resolution TEM images of NiCo/$NiCoO_x$ nanohybrid.

spectra of both $Ni_xCo_{3-x}O_4$ and NiCo/$NiCoO_x$. Two core-level signals of Ni^{2+} centered at ~855.2 and ~872.6 eV were assigned to the Ni^{2+} $2p_{3/2}$ and Ni^{2+} $2p_{1/2}$, respectively.[31,32] Signals located at ~861.2 and ~879.5 eV were the satellite peaks corresponding to Ni^{2+} $2p_{3/2}$ and Ni^{2+} $2p_{1/2}$, respectively.[32] Figure 2C displays the Co 2p core-level XPS spectra. The two primary peaks from Co in $Ni_xCo_{3-x}O_4$ are the typical characteristics of Co 2p1/2 (795.0 eV) and Co p3/2 (779.8 eV) in Co_3O_4.[21,33] However, the two main peaks in the Co 2p core-level XPS spectrum of NiCo/$NiCoO_x$ shifted to higher binding energies compared to $Ni_xCo_{3-x}O_4$. The higher binding energies (796.0 and 780.7 eV) suggested that more Co^{2+} ions were likely generated in NiCo/$NiCoO_x$ owing to the hydrogen reduction.[34,35] Therefore, the slightly shifted signals in the Ni and Co 2p spectra of NiCo/$NiCoO_x$ may be caused by the more complicated surface composition, where Ni and Co may have different valence states derived from hydrogen reduction. Given that XPS can only probe the chemical information within a few atomic layers near the surface, it thus confirmed that the NiCo/$NiCoO_x$ has a crystalline NiCo core and an amorphous $NiCoO_x$ shell. The O 1s XPS spectra were shown in Figure 2D. The O 1s peaks located at ~529.4 and 531.2 eV were attributed to the lattice O^{2-} and oxygen vacancies and/or hydroxyl groups, respectively.[33,36] Obviously, the lattice O^{2-} atoms diminished after hydrogenation as evidenced by the obviously weakened XPS peak intensity, indicating the degradation of the crystal structure. This was consistent with the observations for hydrogenated nickel oxide and cobalt oxide in previous studies.[3,27]

The OER activity of $Ni_xCo_{3-x}O_4$ nanowires and NiCo/$NiCoO_x$ nanohybrid was investigated in a standard three-electrode system using linear sweep voltammetry. For comparison, the OER performances of bare Ni foam and IrO_2 were evaluated under similar conditions. Figure 3A shows the polarization curves of $Ni_xCo_{3-x}O_4$ nanowires, NiCo/$NiCoO_x$ nanohybrid, IrO_2 and Ni foam in 1.0 M KOH at a scan rate of 5 mV s^{-1}. The $Ni_xCo_{3-x}O_4$ nanowires showed an onset of ~1.51 V versus RHE, and required an overpotential of ~337 mV to drive a cathodic current density of 10 mA cm^{-2}. The NiCo/$NiCoO_x$ nanohybrid presented a slightly lower activity with an overpotential of 361 mV at 10 mA cm^{-2} maybe

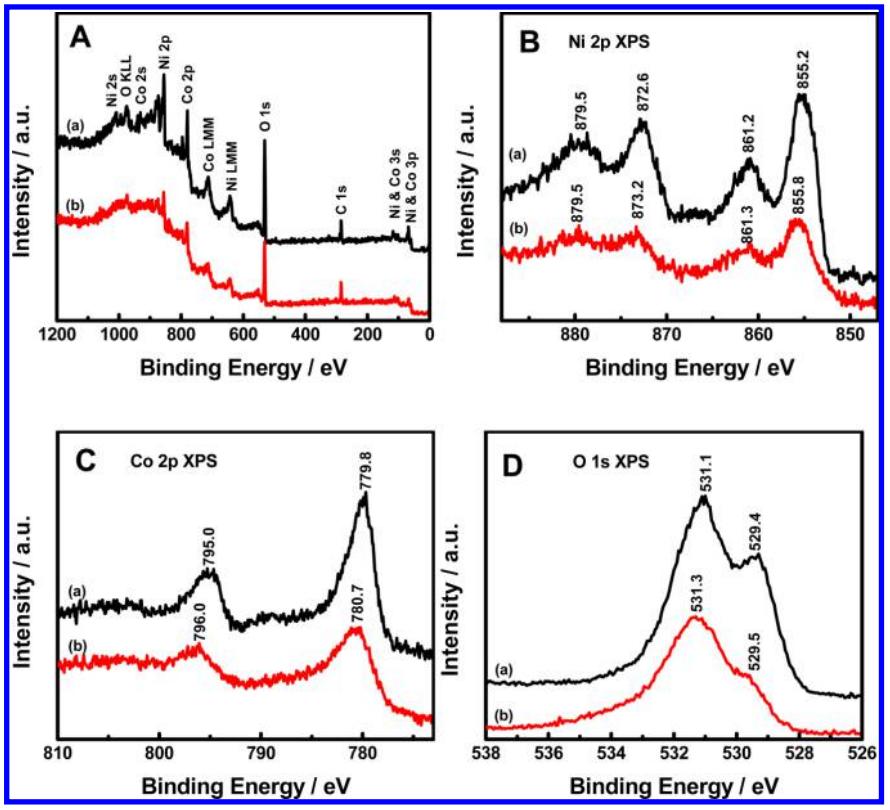

Figure 2. (A) XPS survey and XPS spectra of the (B) Ni 2p, (C) Co 2p, and (D) O 1s peaks of (a) $Ni_xCo_{3-x}O_4$ and (b) NiCo/$NiCoO_x$.

DOI: 10.1021/acsami.5b10724
ACS Appl. Mater. Interfaces 2016, 8, 3208−3214

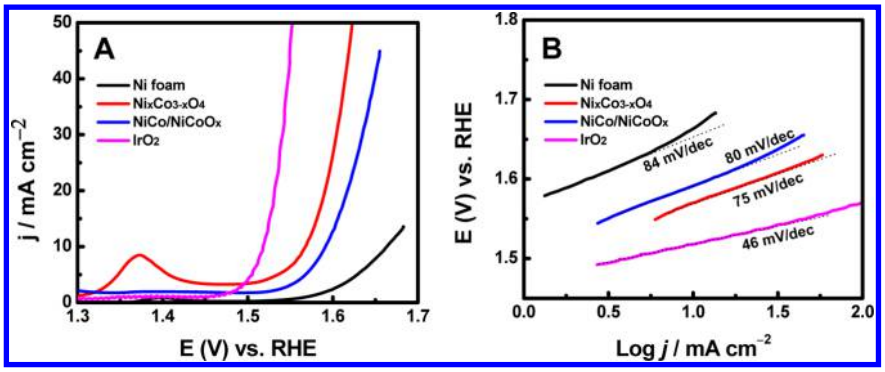

Figure 3. Electrochemical characterizations for OER activity. (A) Polarization curves of $Ni_xCo_{3-x}O_4$ nanowires, $NiCo/NiCoO_x$ nanohybrid, IrO_2 and Ni foam in 1.0 M KOH. (B) Tafel plots derived from panel A.

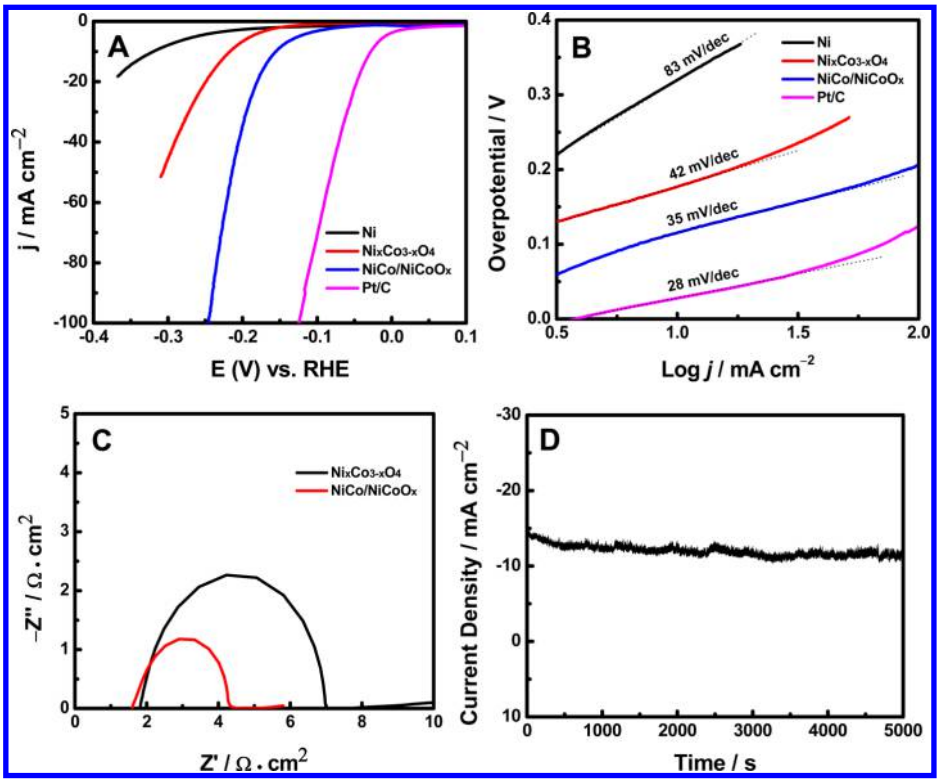

Figure 4. Electrochemical characterizations for HER activity. (A) Polarization curves of various electrodes in 1.0 M KOH. (B) Tafel plots derived from Figure 4A. (C) Nyquist plots of $Ni_xCo_{3-x}O_4$ nanowires and $NiCo/NiCoO_x$ nanohybrid obtained at a potential of −1.2 V versus RHE. (D) Chronopotentiometry curve of $NiCo/NiCoO_x$ nanohybrid without *iR* compensation.

owing to the rapid depletion of the $Ni_xCo_{3-x}O_4$ during the hydrogen reduction. Figure 3B displays the Tafel plots of $Ni_xCo_{3-x}O_4$ nanowires, $NiCo/NiCoO_x$ nanohybrid, IrO_2 and Ni foam derived from Figure 3A. $Ni_xCo_{3-x}O_4$ nanowires presented a lower Tafel slope (75 mV dec^{-1}) than $NiCo/NiCoO_x$ nanohybrid (80 mV dec^{-1}) and Ni foam (84 mV dec^{-1}), indicating faster OER kinetics on the surface of the $Ni_xCo_{3-x}O_4$ nanowire electrode.[37] In conclusion, this performance is better than many of the reported Co_3O_4- and $Ni_xCo_{3-x}O_4$-based catalysts.[37−40] This can be attributed to (1) the three-dimensional nature of our electrode and open space between nanowires which can facilitate the diffusion of electrolyte and oxygen bubbles; (2) the large surface area associated with the nanostructured nanowires along with the absence of binder, accelerating the surface reaction; and (3) the direct contact of nanowires to the underneath conductive substrate which ensures each nanowire to participate in the reaction.[12,41]

The HER activity of $NiCo/NiCoO_x$ nanohybrid was first studied in a standard three-electrode system using liner sweep voltammetry. Bare Ni foam, $Ni_xCo_{3-x}O_4$ nanowires and commercial Pt/C were also comparatively tested under similar conditions. Figure 4A shows the polarization curves of various electrodes in 1.0 M KOH at a scan rate of 5 mV s^{-1}. $NiCo/NiCoO_x$ nanohybrid nanowires showed an onset of −0.065 V versus RHE, whereas it was −0.138 V versus RHE for $Ni_xCo_{3-x}O_4$ nanowires. A small overpotential (~155 mV) was needed for $NiCo/NiCoO_x$ nanohybrid to reach a cathodic current density of 10 mA cm^{-2}, which was 60 mV smaller than that of $Ni_xCo_{3-x}O_4$ nanowires. The much higher HER activity of $NiCo/NiCoO_x$ nanohybrid compared to $Ni_xCo_{3-x}O_4$ nanowires was ascribed to the exposed $NiCo/NiCoO_x$ interface where there was a synergistic effect between metal and metal

DOI: 10.1021/acsami.5b10724
ACS Appl. Mater. Interfaces 2016, 8, 3208−3214

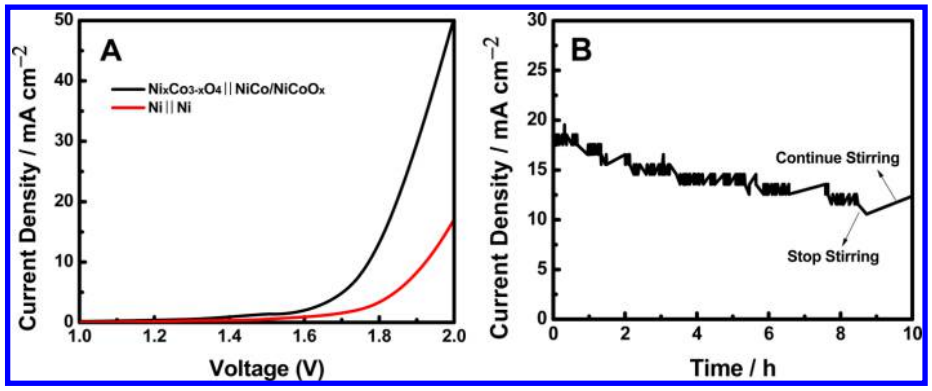

Figure 5. Overall water-splitting characteristics of the $Ni_xCo_{3-x}O_4$ || $NiCo/NiCoO_x$ and Ni || Ni systems in two-electrode configurations in 1 M KOH. All the data are without *i*R compensation. (A) Polarization curves at a scant rate of 5 mV s^{-1}. (B) Current−time characteristics of the $Ni_xCo_{3-x}O_4$ || $NiCo/NiCoO_x$ system at a voltage of 1.80 V.

oxide.[3,21,22,27] In detail, surface amorphous $NiCoO_x$ could facilitate both Volmer and Heyrovesky processes due to its good interaction with OH^- groups;[3,27] NiCo alloy not only improved the conductivity of the catalyst and facilitated the electron transfer but also accelerated the electrochemical reduction of the absorbed H_2O as both Ni and Co were calculated to have suitable H binding energies.[21,22] Figure 4B displays the Tafel plots derived from the polarization curves in Figure 4A. According to the Tafel equation ($\eta = a + b\log|j|$), the Tafel slope (b) describes the current density (j) enhancement versus overpotential (η) in the Tafel region, and the smaller the Tafel slope is, the faster the current density increase with overpotential will be.[42] $NiCo/NiCoO_x$ nanohybrid had a much smaller Tafel slope (35 mV dec^{-1}) than $Ni_xCo_{3-x}O_4$ nanowires (42 mV dec^{-1}), confirming the enhanced HER activity of $NiCo/NiCoO_x$ nanohybrid. To reveal the kinetics on the surface of the electrodes, Nyquist plots were obtained by EIS measurement at a constant potential of −1.2 V versus RHE. One semicircle suggested a one-time-constant behavior for both $Ni_xCo_{3-x}O_4$ nanowires and $NiCo/NiCoO_x$ nanohybrid (Figure 4C).[43] Obviously, the $NiCo/NiCoO_x$ nanohybrid electrode had a much smaller charge transfer resistance (2.8 Ω) than that of $Ni_xCo_{3-x}O_4$ nanowire electrode (5.2 Ω). This indicated a faster charge transfer process or a faster hydrogen evolution rate on the surface of the $NiCo/NiCoO_x$ electrode,[43,44] which was solid evidence of the synergistic effect of the highly conductive NiCo core and the amorphouos $NiCoO_x$ shell. The stability of $NiCo/NiCoO_x$ nanohybrid was evaluated using constant voltage technique. At a constant overpotential of 200 mV, the current showed slight degradation during a long period of 6000 s (Figure 4D). This indicated a good stability of the $NiCo/NiCoO_x$ nanohybrid as HER catalyst.

An electrolyzer with $Ni_xCo_{3-x}O_4$ nanowires and $NiCo/NiCoO_x$ nanohybrid as the anode and cathode electrodes was assembled to demonstrate the overall water splitting activity in 1 M KOH. The liner sweep voltammetry of the $Ni_xCo_{3-x}O_4$ || $NiCo/NiCoO_x$ system showed that the electrolysis process proceeded at an applied potential of 1.58 V (Figure 5A). A current density of 10 mA cm^{-2} was achieved at a voltage of ∼1.75 V (Figure 5A), corresponding to an overpotential of 520 mV. In sharp comparison, the Ni || Ni system required an overpotential of 690 mV to reach 10 mA cm^{-2}. The durability of the electrolyzer, which is of great importance for the practical applications, was carried at 1.8 V in 1 M KOH at room temperature. The HER current gradually decreased from 18 to 12 mA cm^{-2} after water electrolysis for 10 h (Figure 5B). The current decrease was more likely caused by the limited mass transfer, as the stirring greatly affected the current and the polarization curves before and after the long-term stability showed negligible change (Figure S6). This indicated that the as-prepared catalysts had a good stability. These results indicated that our $Ni_xCo_{3-x}O_4$ || $NiCo/NiCoO_x$ system is a promising candidate for water splitting owing to their high electrocatalytic activity, excellent stability, and simple synthesis.

4. CONCLUSIONS

In summary, we have developed a low-cost, earth-abundant catalyst pair composed of $Ni_xCo_{3-x}O_4$ nanowires and $NiCo/NiCoO_x$ nanohybrid for overall water splitting, acting as OER catalyst and HER catalyst, respectively. $NiCo/NiCoO_x$ nanohybrid can be readily achieved from $Ni_xCo_{3-x}O_4$ nanowires through a simple hydrogen reduction process at a relatively low temperature, achieving the transformation from OER catalyst to HER catalyst. $NiCo/NiCoO_x$ nanohybrid demonstrates a high catalytic activity toward HER with a small onset overpotential of 65 mV due to the synergistic effect between metal and amorphous metal oxide. More importantly, when assembled in an alkaline electrolyzer, the catalyst pair exhibits both high activity and robust stability. Therefore, we demonstrate a new way of tuning the HER-OER performance of electrocatalysts through the structural modification with hydrogenation for overall water splitting.

■ ASSOCIATED CONTENT

Supporting Information

The Supporting Information is available free of charge on the ACS Publications website at DOI: 10.1021/acsami.5b10724.

(PDF)

■ AUTHOR INFORMATION

Corresponding Author

*E-mail: chenxiaobo@umkc.edu.

Notes

The authors declare no competing financial interest.

■ ACKNOWLEDGMENTS

X.C. acknowledges the support from College of Arts and Sciences, University of Missouri, Kansas City, the University of Missouri Research Board (UMRB) and the University of Missouri Interdisciplinary Intercampus (IDIC) Programs. L.L.

DOI: 10.1021/acsami.5b10724
ACS Appl. Mater. Interfaces 2016, 8, 3208−3214

and J.H. acknowledge the support of the National Natural Science Foundation of China (Nos. 11174273 and 11174371).

REFERENCES

(1) Chen, X.; Liu, L.; Yu, P. Y.; Mao, S. S. Increasing Solar Absorption for Photocatalysis with Black Hydrogenated Titanium Dioxide Nanocrystals. *Science* **2011**, *331*, 746−750.

(2) Chen, X.; Shen, S.; Guo, L.; Mao, S. S. Semiconductor-based Photocatalytic Hydrogen Generation. *Chem. Rev.* **2010**, *110*, 6503−6570.

(3) Yan, X.; Tian, L.; He, M.; Chen, X. Three-Dimensional Crystalline/Amorphous Co/Co_3O_4 Core/Shell Nanosheets as Efficient Electrocatalysts for the Hydrogen Evolution Reaction. *Nano Lett.* **2015**, *15*, 6015−6021.

(4) Kong, D.; Wang, H.; Lu, Z.; Cui, Y. $CoSe_2$ Nanoparticles Grown on Carbon Fiber Paper: An Efficient and Stable Electrocatalyst for Hydrogen Evolution Reaction. *J. Am. Chem. Soc.* **2014**, *136*, 4897−4900.

(5) Zhou, W.; Li, W.; Wang, J.-Q.; Qu, Y.; Yang, Y.; Xie, Y.; Zhang, K.; Wang, L.; Fu, H.; Zhao, D. Ordered Mesoporous Black TiO_2 as Highly Efficient Hydrogen Evolution Photocatalyst. *J. Am. Chem. Soc.* **2014**, *136*, 9280−9283.

(6) Liu, N.; Schneider, C.; Freitag, D.; Hartmann, M.; Venkatesan, U.; Müller, J.; Spiecker, E.; Schmuki, P. Black TiO_2 Nanotubes: Cocatalyst-Free Open-Circuit Hydrogen Generation. *Nano Lett.* **2014**, *14*, 3309−3313.

(7) Luo, J.; Im, J.-H.; Mayer, M. T.; Schreier, M.; Nazeeruddin, M. K.; Park, N.-G.; Tilley, S. D.; Fan, J. F.; Grätzel, M. Water Photolysis at 12.3% Efficiency via Perovskite Photovoltaics and Earth-Abundant Catalysts. *Science* **2014**, *345*, 1593−1596.

(8) Stern, L.-A.; Hu, X. Enhanced Oxygen Evolution Activity by NiO_x and $Ni(OH)_2$ Nanoparticles. *Faraday Discuss.* **2014**, *176*, 363−379.

(9) Tian, J.; Liu, Q.; Liang, Y.; Xing, Z.; Asiri, A. M.; Sun, X. FeP Nanoparticles Film Grown on Carbon Cloth: An Ultrahighly Active 3D Hydrogen Evolution Cathode in Both Acidic and Neutral Solutions. *ACS Appl. Mater. Interfaces* **2014**, *6*, 20579−20584.

(10) Kong, D.; Cha, J. J.; Wang, H.; Lee, H. R.; Cui, Y. First-Row Transition Metal Dichalcogenide Catalysts for Hydrogen Evolution Reaction. *Energy Environ. Sci.* **2013**, *6*, 3553−3558.

(11) Liu, Y.; Wang, H.; Lin, D.; Liu, C.; Hsu, P.-C.; Liu, W.; Chen, W.; Cui, Y. Electrochemical Tuning of Olivine-Type Lithium Transition-Metal Phosphates as Efficient Water Oxidation Catalysts. *Energy Environ. Sci.* **2015**, *8*, 1719−1724.

(12) Lu, Z.; Xu, W.; Zhu, W.; Yang, Q.; Lei, X.; Liu, J.; Li, Y.; Sun, X.; Duan, X. Three-Dimensional NiFe Layered Double Hydroxide Film for High-Efficiency Oxygen Evolution Reaction. *Chem. Commun.* **2014**, *50*, 6479−6482.

(13) Qian, L.; Lu, Z.; Xu, T.; Wu, X.; Tian, Y.; Li, Y.; Huo, Z.; Sun, X.; Duan, X. Trinary Layered Double Hydroxides as High-Performance Bifunctional Materials for Oxygen Electrocatalysis. *Adv. Energy Mater.* **2015**, *5*, 1500245.

(14) Callejas, J. F.; McEnaney, J. M.; Read, C. G.; Crompton, J. C.; Biacchi, A. J.; Popczun, E. J.; Gordon, T. R.; Lewis, N. S.; Schaak, R. E. Electrocatalytic and Photocatalytic Hydrogen Production from Acidic and Neutral-pH Aqueous Solutions Using Iron Phosphide Nanoparticles. *ACS Nano* **2014**, *8*, 11101−11107.

(15) Popczun, E. J.; McKone, J. R.; Read, C. G.; Biacchi, A. J.; Wiltrout, A. M.; Lewis, N. S.; Schaak, R. E. Nanostructured Nickel Phosphide as an Electrocatalyst for the Hydrogen Evolution Reaction. *J. Am. Chem. Soc.* **2013**, *135*, 9267−9270.

(16) Tian, J.; Liu, Q.; Asiri, A. M.; Sun, X. Self-Supported Nanoporous Cobalt Phosphide Nanowire Arrays: An Efficient 3D Hydrogen-Evolving Cathode over the Wide Range of pH 0−14. *J. Am. Chem. Soc.* **2014**, *136*, 7587−7590.

(17) Liu, Q.; Tian, J.; Cui, W.; Jiang, P.; Cheng, N.; Asiri, A. M.; Sun, X. Carbon Nanotubes Decorated with CoP Nanocrystals: A Highly Active Non-Noble-Metal Nanohybrid Electrocatalyst for Hydrogen Evolution. *Angew. Chem.* **2014**, *126*, 6828−6832.

(18) Gong, M.; Li, Y.; Wang, H.; Liang, Y.; Wu, J. Z.; Zhou, J.; Wang, J.; Regier, T.; Wei, F.; Dai, D. An Advanced Ni−Fe Layered Double Hydroxide Electrocatalyst for Water Oxidation. *J. Am. Chem. Soc.* **2013**, *135*, 8452−8455.

(19) Song, F.; Hu, X. Exfoliation of Layered Double Hydroxides for Enhanced Oxygen Evolution Catalysis. *Nat. Commun.* **2014**, *5*, 4477.

(20) Liang, H.; Meng, F.; Cabán-Acevedo, M.; Li, L.; Forticaux, A.; Xiu, L.; Wang, Z.; Jin, S. Hydrothermal Continuous Flow Synthesis and Exfoliation of NiCo Layered Double Hydroxide Nanosheets for Enhanced Oxygen Evolution Catalysis. *Nano Lett.* **2015**, *15*, 1421−1427.

(21) Jin, H.; Wang, J.; Su, D.; Wei, Z.; Pang, Z.; Wang, Y. In situ Cobalt−Cobalt Oxide/N-doped Carbon Hybrids as Superior Bifunctional Electrocatalysts for Hydrogen and Oxygen Evolution. *J. Am. Chem. Soc.* **2015**, *137*, 2688−2694.

(22) Gong, M.; Zhou, W.; Tsai, M.-C.; Zhou, J.; Guan, M.; Lin, M.-C.; Zhang, B.; Hu, Y.; Wang, D.-Y.; Yang, J.; Pennycook, S. J.; Hwang, B.-J.; Dai, H. Nanoscale Nickel Oxide/Nickel Heterostructures for Active Hydrogen Evolution Electrocatalysis. *Nat. Commun.* **2014**, *5*, 4695.

(23) Wang, H.; Lee, H.-W.; Deng, Y.; Lu, Z.; Hsu, P.-C.; Liu, Y.; Lin, D.; Cui, Y. Bifunctional Non-Noble Metal Oxide Nanoparticle Electrocatalysts Through Lithium-Induced Conversion for Overall Water Splitting. *Nat. Commun.* **2015**, *6*, 7261.

(24) Wang, H.; Lu, Z.; Kong, D.; Sun, J.; Hymel, T. M.; Cui, Y. Electrochemical Tuning of MoS_2 Nanoparticles on Three-Dimensional Substrate for Efficient Hydrogen Evolution. *ACS Nano* **2014**, *8*, 4940−4947.

(25) Wang, H.; Lu, Z.; Xu, S.; Kong, D.; Cha, J. J.; Zheng, G.; Hsu, P.-C.; Yan, K.; Bradshaw, D.; Prinz, F. B.; Cui, Y. Electrochemical Tuning of Vertically Aligned MoS_2 Nanofilms and Its Application in Improving Hydrogen Evolution Reaction. *Proc. Natl. Acad. Sci. U. S. A.* **2013**, *110*, 19701−19706.

(26) Lu, Z.; Wang, H.; Kong, D.; Yan, K.; Hsu, P.-C.; Zheng, G.; Yao, H.; Liang, Z.; Sun, X.; Cui, Y. Electrochemical Tuning of Layered Lithium Transition Metal Oxides for Improvement of Oxygen Evolution Reaction. *Nat. Commun.* **2014**, *5*, 4345.

(27) Yan, X.; Tian, L.; Chen, X. Crystalline/Amorphous Ni/NiO Core/Shell Nanosheets as Highly active Electrocatalysts for Hydrogen Evolution Reaction. *J. Power Sources* **2015**, *300*, 336−343.

(28) Li, Y. H.; Liu, P. F.; Pan, L. F.; Wang, H. F.; Yang, Z. Z.; Zheng, L. R.; Hu, P.; Zhao, H. J.; Gu, L.; Yang, H. G. Local Atomic Structure Modulations Activate Metal Oxide as Electrocatalyst for Hydrogen Evolution in Acidic Water. *Nat. Commun.* **2015**, *6*, 8064.

(29) Xia, T.; Zhang, W.; Wang, Z.; Zhang, Y.; Song, X.; Murowchick, J.; Battaglia, V.; Liu, G.; Chen, X. Amorphous Carbon-Coated TiO_2 Nanocrystals for Improved Lithium-Ion Battery and Photocatalytic Performance. *Nano Energy* **2014**, *6*, 109−118.

(30) Wei, X.-W.; Zhou, X.-M.; Wu, K.-L.; Chen, Y. 3-D Flower-Like NiCo Alloy Nano/Microstructures Grown by A Surfactant-Assisted Solvothermal Process. *CrystEngComm* **2011**, *13*, 1328−1332.

(31) Lian, K. K.; Kirk, D. W.; Thorpe, S. J. Investigation of a "Two-State" Tafel Phenomenon for the Oxygen Evolution Reaction on an Amorphous Ni-Co Alloy. *J. Electrochem. Soc.* **1995**, *142*, 3704−3712.

(32) Mansour, A. Characterization of NiO by XPS. *Surf. Sci. Spectra* **1994**, *3*, 231−238.

(33) Xia, H.; Zhu, D.; Luo, Z.; Yu, Y.; Shi, X.; Yuan, G.; Xie, J. Hierarchically Structured Co_3O_4@Pt@MnO_2 Nanowire Arrays for High-Performance Supercapacitors. *Sci. Rep.* **2013**, *3*, 2978.

(34) Tan, B. J.; Klabunde, K. J.; Sherwood, P. M. A. XPS Studies of Solvated Metal Atom Dispersed (SMAD) Catalysts. Evidence for Layered Cobalt-Manganese Particles on Alumina and Silica. *J. Am. Chem. Soc.* **1991**, *113*, 855.

(35) Nefedov, V. I.; Firsov, M. N.; Shaplygin, I. S. Electronic Structures of $MRhO_2$, MRh_2O_4, $RhMO_4$ and Rh_2MO_6 on the Basis of X-ray Spectroscopy and ESCA Data. *J. Electron Spectrosc. Relat. Phenom.* **1982**, *26*, 65.

DOI: 10.1021/acsami.5b10724
ACS Appl. Mater. Interfaces 2016, 8, 3208−3214

(36) Zhang, X.; Qin, J.; Xue, Y.; Yu, P.; Zhang, B.; Wang, L.; Liu, R. Effect of Aspect Ratio and Surface Defects on the Photocatalytic Activity of ZnO Nanorods. *Sci. Rep.* **2014**, *4*, 4596.
(37) Xiao, C.; Lu, X.; Zhao, C. Unusual Synergistic Effects upon Incorporation of Fe and/or Ni into Mesoporous Co_3O_4 for Enhanced Oxygen Evolution. *Chem. Commun.* **2014**, *50*, 10122−10125.
(38) Yu, X.; Sun, Z.; Yan, Z.; Xiang, B.; Liu, X.; Du, P. Direct Growth of Porous Crystalline $NiCo_2O_4$ Nanowire Arrays on A Conductive Electrode for High-Performance Electrocatalytic Water Oxidation. *J. Mater. Chem. A* **2014**, *2*, 20823−20831.
(39) Zhou, X.; Xia, Z.; Tian, Z.; Ma, Y.; Qu, Y. Ultrathin Porous Co_3O_4 Nanoplates as Highly Efficient Oxygen Evolution Catalysts. *J. Mater. Chem. A* **2015**, *3*, 8107−8114.
(40) Zhao, J.; Zou, Y.; Zou, X.; Bai, T.; Liu, Y.; Gao, R.; Wang, D.; Li, G.-D. Self-Template Construction of Hollow Co_3O_4 Microspheres from Porous Ultrathin Nanosheets and Efficient Noble Metal-Free Water Oxidation Catalysts. *Nanoscale* **2014**, *6*, 7255−7262.
(41) Peng, Z.; Jia, D.; Al-Enizi, A. M.; Elzatahry, A. A.; Zheng, G. From Water Oxidation to Reduction: Homologous Ni−Co Based Nanowires as Complementary Water Splitting Electrocatalysts. *Adv. Energy Mater.* **2015**, *5*, 1402031.
(42) Geng, J.; Kuai, L.; Kan, E.; Wang, Q.; Geng, B. Precious-Metal-Free Co−Fe−O/rGO Synergetic Electrocatalysts for Oxygen Evolution Reaction by a Facile Hydrothermal Route. *ChemSusChem* **2015**, *8*, 659−664.
(43) Yan, Y.; Thia, L.; Xia, B. Y.; Ge, X.; Liu, Z.; Fisher, A.; Wang, X. Construction of Efficient 3D Gas Evolution Electrocatalyst for Hydrogen Evolution: Porous FeP Nanowire Arrays on Graphene Sheets. *Adv. Sci.* **2015**, *2*, 1500120.
(44) Xie, J.; Zhang, H.; Li, S.; Wang, R.; Sun, X.; Zhou, M.; Zhou, J.; Lou, X. W.; Xie, Y. Defect-Rich MoS_2 Ultrathin Nanosheets with Additional Active Edge Sites for Enhanced Electrocatalytic Hydrogen Evolution. *Adv. Mater.* **2013**, *25*, 5807.

DOI: 10.1021/acsami.5b10724
ACS Appl. Mater. Interfaces 2016, 8, 3208−3214